ACS OMEGA

Article

Cite This: ACS Omega 2018, 3, 6217−6223

Dandelion-Like Microspherical MCM-22 Zeolite Using BP 2000 as a Hard Template

Anderson Schwanke,*[,†,∥] Jhonny Villarroel-Rocha,[‡] Karim Sapag,[‡] Urbano Díaz,[§] Avelino Corma,[§] and Sibele Pergher[∥]

[†]Departamento de Química, Laboratório de Reatividade e Catálise, Universidade Federal do Rio Grande do Sul, 9500, 91540-000 Porto Alegre, Rio Grande do Sul, Brasil

[‡]Laboratorio de Sólidos Porosos, Universidad Nacional de San Luis, Instituto de Física Aplicada, 5700, D5700BPB San Luis, Argentina

[§]Instituto de Tecnología Química, Universitat Politècnica de València-Consejo-Superior de Investigaciones Científicas (UPV-CSIC), s/n, 46022 Valencia, Spain

[∥]Instituto de Química, Laboratório de Peneiras Moleculares (LABPEMOL), Universidade Federal do Rio Grande do Norte, 3000, 59078-970 Natal, Rio Grande do Norte, Brasil

Supporting Information

ABSTRACT: The chemistry between layered MWW zeolite and carbon black pearls (BP 2000) as an inexpensive hard template was investigated to develop a rational one-pot synthesis of MCM-22 microspheres. The characterization results showed that the insertion of BP 2000 in the gel synthesis did not substantially compromise the crystallinity and microporosity, and the microscopic analyses showed that BP 2000 played a key role in controlling the final morphology of the MCM-22 zeolite, creating beautiful dandelion-like microspherical particles. The morphology obtained is due to the tortuous shape of the hard template, the particular MWW particle crystals, the interaction with the external surface of the MWW zeolitic precursor, and the synthesis conditions. The stacking of MWW crystals with edge-to-face orientations generates meso-/macrovoids, allowing access to the interiors of the microspheres. The microspheres were homogeneous with sizes ranging from 6 to 8 μm with an increase of the external surface and a macroporous size distribution centered at 200 nm, which is two times that of the traditional MCM-22 zeolite.

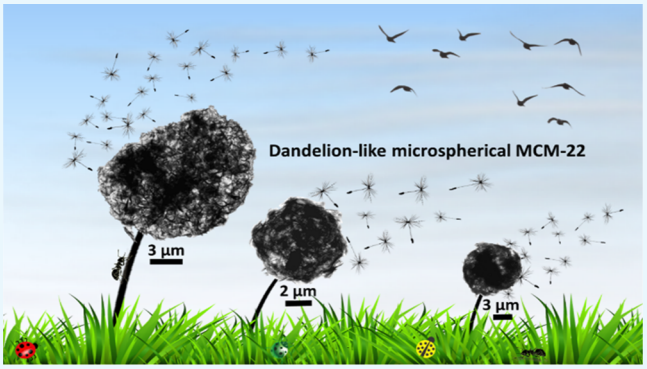

INTRODUCTION

Zeolites play key roles in a variety of processes, for example, adsorption, molecular sieving, ion exchange, and catalysis.[1,2] Recently, zeolites have been applied to new fields, including medicine, cosmetics, food industry, microelectronics, and luminescence.[3,4] This versatility is due to their microporous crystalline nature composed of SiO_4 and AlO_4 tetrahedral coordinated by oxygen atoms. The organization of these tetrahedral units generates porous structures with different types of cavities and channels.

In the last few years, much effort has been given to increase the efficiencies of zeolite-based catalysts.[5] As an example, to improve the physicochemical properties of materials, additional intracrystalline and/or intercrystalline porosity was introduced to achieve shorter diffusion pathways to facilitate the transport of bulky reactants and products.[6] In addition, adapting zeolites and catalysts in hollow, nano-, and microspherical morphologies is still an emerging and innovative field of materials chemistry.[7,8] The construction of a large internal void and its capacity to capsule molecules or nanoparticles serving as nanoreactors for catalytic reactions, drug/gene delivery, or medical imaging has been of considerable interest during the last few decades.[9−11] Furthermore, if the catalytic activity is not compromised, controlling large-sized catalyst particles may be favorable for recyclability of the catalyst in reaction media by filtration or centrifugation processes.[12]

Among the two main strategies, the "bottom-up" and "top-down" approaches, to modify zeolites, bottom-up approaches make use of soft or hard templates to generate hierarchical zeolites.[13] Typically, soft-templating approaches use cationic surfactants,[14] whereas hard-templating approaches utilize carbon particles,[15] polymers,[16,17] bacteria,[18] rice husks,[19] starches,[20] diatomite,[21] $CaCO_3$,[22] or mesoporous silica particles.[23]

Received: April 4, 2018
Accepted: May 25, 2018
Published: June 11, 2018

DOI: 10.1021/acsomega.8b00647
ACS Omega 2018, 3, 6217−6223

Specifically, carbon particles are a class of materials that include carbon spheres, nanotubes, carbon mesostructures from Korea (CMK), and three-dimensionally ordered macroporous carbon replicas.[24−28] Whereas carbon nanotubes are still expensive to use as hard templates, carbon spheres, such as carbon black pearls 2000 (BP 2000), are an inexpensive source of carbon obtained by an incomplete combustion of aromatic petroleum residues.[29] The average carbon particles (12 nm) are tortuous aggregates, which form agglomerated carbon particles.[26] Their use in the synthesis of zeolites by steam-assisted and static crystallization procedures has been reported to produce hierarchical MFI (Mobil Five) mesoporous-type zeolites and MFI zeolites with meso- and macrovoids, respectively.[24,30] However, in the latter case, inhomogeneous and nonspherical particles are formed.

The use of BP 2000 has been widespread for the synthesis of other zeolites, for example, ZSM-12, ZSM-11, and TS-1.[31,32] Additionally, BP 2000 has been used to produce small crystals by confined space synthesis, where the porous and inert matrix of carbon dictates the crystal size generated in the synthesis. Indeed, after removal of the carbon matrix, very small crystals are formed with high crystallinity for ZSM-5, beta, X, and zeolite A.[33,34] To the best of our knowledge, these have been the only studies to utilize BP 2000 as a hard template.

Moreover, much effort has been made to modify the morphologies and properties of zeolites with layered structures.[35−37] Indeed, layered zeolites are considered the most promising materials to replace the currently used catalysts and advance the areas of study on porous and hierarchical materials.[35] Among layered zeolites, the MWW precursor is widely versatile in generating materials with different pore architectures, for example, pillared, delaminated, and disordered.[38−40] However, all these procedures have focused on soft-templating approaches. As the chemistry between layered MWW zeolites and hard templates is relatively unknown, we explored, for the first time, the utilization of BP 2000 as an inexpensive hard template in the traditional synthesis of MCM-22 by a one-pot approach.

RESULTS AND DISCUSSION

The X-ray diffraction (XRD) patterns of traditional (P)MCM-22 and the precursor with BP 2000 ((P)MCM-22-BP) and calcined MCM-22-BP are shown in Figure 1. For both MWW precursors, the diffraction peaks showed the same intensities, which indicates that BP 2000 insertion did not compromise the crystallinity. The diffraction bands located at 2θ = 6.6° correspond to the (002) plane relative to the MWW zeolitic layer stacking with a *d*-spacing of 2.6 nm. These layers are connected by hydrogen bonds between the silanol groups, and the hexamethyleneimine (HMI) template molecules are located between the layers. After calcination, the silanol groups were condensed together with the elimination of the interlayer organic template, leading to the three-dimensional MCM-22-BP zeolite. In addition, intralayer diffraction bands located at 2θ = 7.1° correspond to the (100) plane, and reflections at higher 2θ angles of 25.1° and 26.2° are assigned to the (220) and (310) planes, respectively. The obtained product (P)MCM-22-BP showed a yield of 100%, which is similar to that of the traditional (P)MCM-22. The dried product (P)MCM-22-BP was a homogeneous white gray color when compared with the common beige color of traditional (P)MCM-22 as shown in Figure 1. This indicates that BP 2000 did not form isolated aggregates in the (P)MCM-22-BP sample.

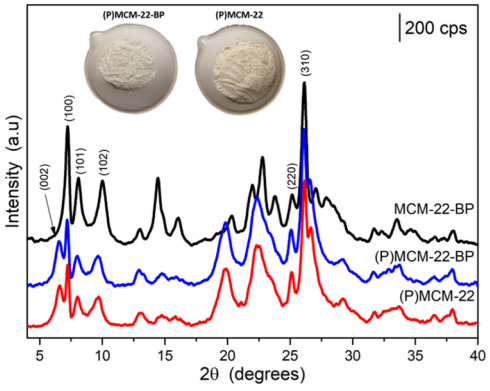

Figure 1. XRD patterns of synthesized (P)MCM-22-BP, calcined MCM-22-BP, and traditional (P)MCM-22

The ICP (inductively coupled plasma) analysis of the calcined materials showed Si/Al molar ratios of 23 and 25 for MCM-22-BP and traditional MCM-22, respectively. Therefore, the insertion of BP 2000 did not affect the crystallization efficiency of aluminum during nucleation. The aluminum in zeolites could occupy framework or extra-framework positions, which correspond to the aluminum in the tetrahedral (Al_{tet}) or octahedral (Al_{oct}) coordination. To distinguish the chemical environment of the aluminum of the samples, Figure 2 shows

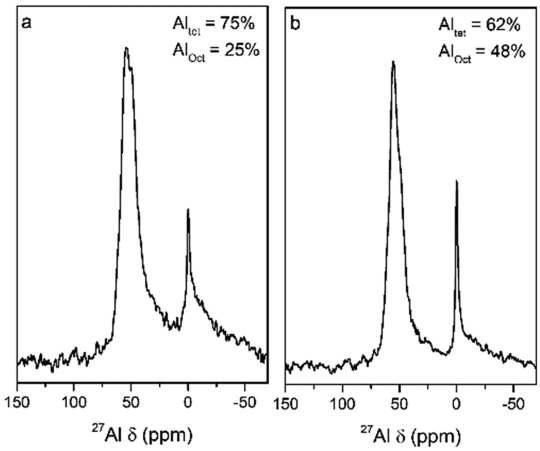

Figure 2. ^{27}Al MAS NMR spectra of MCM-22-BP (a) and traditional MCM-22 (b) samples.

the ^{27}Al MAS (magic-angle spinning) NMR spectra of the MCM-22-BP and traditional MCM-22 zeolites. The signals at ca. 50 ppm are characteristic of Al_{tet}, and the signals at ca. 0 ppm are characteristic of Al_{oct}. It was observed that both samples showed a higher signal at ca. 50 ppm, which corresponded to a higher population of Al_{tet} than Al_{oct}. It was also observed that Al_{tet} in MCM-22-BP has a greater proportion (75%) than in the traditional MCM-22 sample (62%). This difference suggests that the insertion of the black pearls acts in some way to prevent the formation of extra-framework aluminum. However, this hypothesis requires further study.

Nitrogen adsorption−desorption isotherms of the MCM-22 materials are shown in Figure 3 (image a). Both MCM-22 zeolites exhibited type I isotherms, which confirms their microporous nature.[41] However, the adsorption isotherms for

DOI: 10.1021/acsomega.8b00647
ACS Omega 2018, 3, 6217−6223

Table 1. Weight Loss and Elemental Analysis of Precursor and Calcined Products

	weight loss (%)			elemental analysis (%)			
sample	180−480 °C	480−800 °C	total	C	H	N	total
(P)MCM-22-BP	11.00	7.73	18.73	11.70	2.05	1.97	15.72
(P)MCM-22	12.31	5.70	18.01	11.49	1.97	1.99	15.45
MCM-22-BP	1.56	0.95	2.51	0.28	0.48	0.01	0.77
MCM-22	1.26	0.49	1.75	0.15	0.43	0.00	0.58

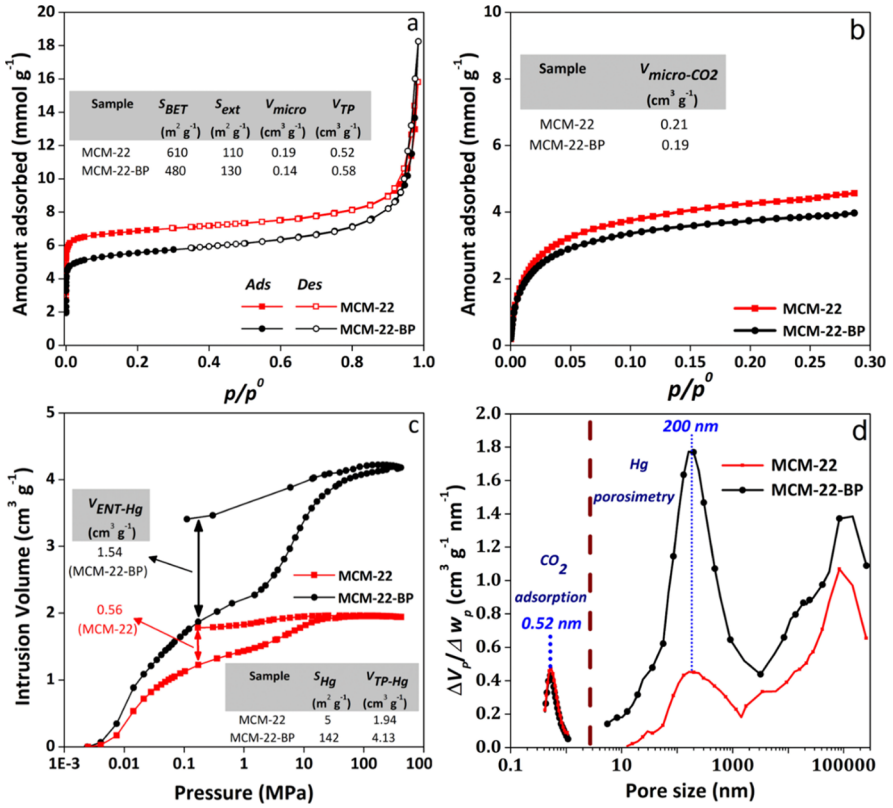

Figure 3. Nitrogen adsorption−desorption isotherms at 77 K (a), carbon dioxide adsorption isotherms at 273 K (b), curves of mercury intrusion−extrusion (c), and pore size distributions of the MCM-22-BP and traditional MCM-22 zeolites (d).

both zeolites showed a quick increase of nitrogen amount adsorbed at relative pressures higher than $p/p^0 = 0.8$, corresponding to the nitrogen adsorption on intercrystalline porosity (larger mesopores or macropores), where the MCM-22-BP sample showed a total pore volume (V_{TP}) value higher than that of the traditional MCM-22 zeolite. The micropore volume (V_{micro}) of MCM-22-BP was 0.14 $cm^3\ g^{-1}$, and that of traditional MCM-22 was 0.19 $cm^3\ g^{-1}$.

The MCM-22 zeolite presents micropores with 0.52 nm, which is in the range of ultramicropores. However, N_2 at −196 °C shows diffusion problems (the adsorption is carried out at a very low temperature), and the correct characterization of the micropores should be with CO_2 as the probe molecule at 0 °C.[42,43] Thus, the characterization of the narrow microporosity with the CO_2 adsorption isotherms of MCM-22-BP and MCM-22 samples are shown in Figure 3 (image b). The shape of the isotherms (such as the type I isotherm) is similar for the two studied zeolites. It was observed that the $V_{micro\text{-}CO_2}$ values of MCM-22-BP and traditional MCM-22 were 0.19 and 0.21 $cm^3\ g^{-1}$, respectively, which are less than the V_{micro} obtained by the N_2 isotherms. The decrease of V_{micro} (for CO_2) of MCM-22-BP when compared to traditional MCM-22 may be attributed to the inhibition of the formation of the microporous structure to some degree and/or the presence of carbon residues in the micropores. Indeed, the weight loss values obtained by thermogravimetric analysis (TGA) in Table 1 show that the weight loss was higher for MCM-22-BP (2.51%) than for traditional MCM-22 (1.75%) at temperatures above 180 °C. In addition, the CHN (carbon, hydrogen, nitrogen) elemental analyses Figure 3 (image d)), which is consistent with the two independent porous systems (bidirectional and sinusoidal) of ten-membered rings of the MWW structure with 0.52 nm of internal diameter. This indicates that BP 2000 insertion did not substantially affect the formation of the microporous structure of the MCM-22-BP zeolite.

Regarding characterization of the macropores, the curves of mercury intrusion−extrusion for both zeolites are shown in Figure 3 (image c). It is possible to observe that the MCM-22-BP presents a mercury intrusion volume two times as high as that of the MCM-22 sample (as reflected in the $V_{TP\text{-}Hg}$ values). The macropore size distribution (right side of Figure 4 (image c)) shows that the macropore population between 50 and 3000 nm (with 200 nm of modal pore size) increased considerably in the MCM-22-BP zeolite with respect to the MCM-22 sample. This result is consistent with the macrovoids shown by the regions with less density contrast in the transmission electron

DOI: 10.1021/acsomega.8b00647
ACS Omega 2018, 3, 6217−6223

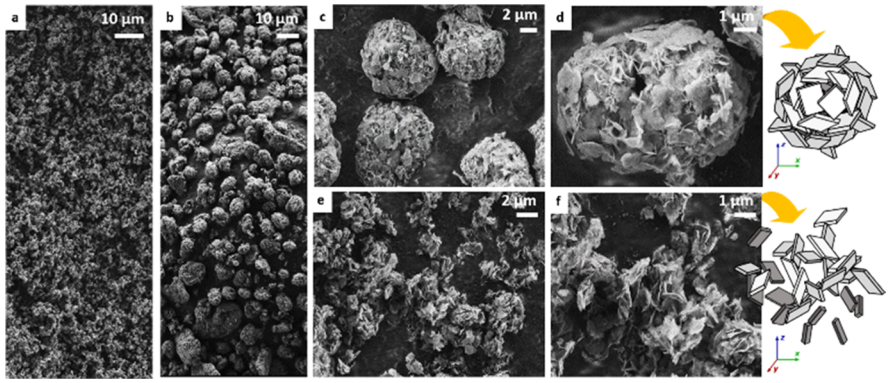

Figure 4. SEM of traditional (P)MCM-22 (a) and (P)MCM-22-BP with a microspherical morphology (b). SEM of traditional MCM-22 (e,f) and MCM-22-BP (c,d) after calcination.

microscopy (TEM) analysis shown in Figures 6 and S1 (image a). In addition, Figure 4 (image c) shows the entrapment level of mercury (V_{ENT-Hg}) for a pore size of 8 μm (corresponding to 0.16 MPa of pressure) for both samples, where MCM-22-BP has an entrapment level three times as high as that of the MCM-22 zeolite. This fact is related to a network of interconnected pores between the macrovoids and their narrow inlets; thus, in the extrusion process, the mercury is trapped in the macrovoids.

Scanning electron microscopy (SEM) analyses in Figure 4 (images a,e,f) show the platelet crystals of the traditional (P)MCM-22 zeolite, and Figure 5 (image b) shows the formation of homogeneous microspherical particles of (P)MCM-22-BP with sizes ranging between 6 and 8 μm, which are maintained after calcination (images c,d). These microspheres are formed by the aggregation of thin MWW crystal platelets stacked in edge-to-face orientations. In addition, macrovoids (see the dark regions in the microspheres in images c,d), which allow access to the microspheres, were also observed. Figure 4 (images e,f) shows the traditional morphology of MCM-22, and its crystalline particles are randomly oriented, which is clearly different from MCM-22-BP.

TEM analysis shows that the MCM-22-BP microspheres are formed by the aggregation of MWW platelets on a beautiful dandelion-like morphology as shown in Figure 5 (images a,b).

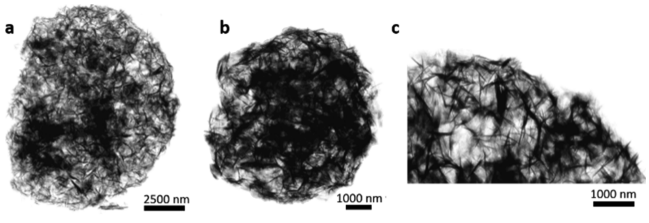

Figure 5. TEM of MCM-22-BP spheres (a,b) and a border region with an edge-to-face orientation of MWW crystals (c).

The spheres were not dense, allowing access to their interiors by macrovoids (image c). We compared the microspherical morphology of the dandelion-like MCM-22-BP zeolite with the doughnut-like morphology of the MCM-22 zeolite obtained under static conditions in Figure 6. It was observed that MCM-22-static (image a) formed large and dense particles with dimensions of 18 μm × 16 μm, which are obtained by the stacking of several MWW crystal platelets in face-to-face orientations. In contrast, the dandelion-like microspheres

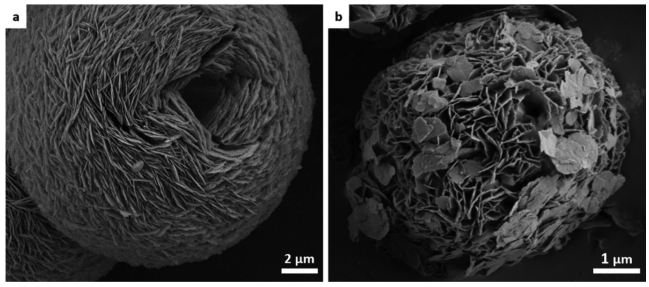

Figure 6. SEM of doughnut-like MCM-22-static (a) and dandelion-like MCM-22-BP sphere (b) morphologies.

(image b) are not a proper hollow-shell structure but consist of edge-to-face orientations of MWW crystal layers in the entire microsphere. The orientation of the crystal layers was reflected in the different S_{ext} values of the samples. The MCM-22-static showed 56 m^2 g^{-1} and the MCM-22-BP showed 130 m^2 g^{-1} (the complete textural properties of the MCM-22-static are shown in Figure S2).

It was reported that carbon black pearl BP 2000 possesses an average particle size of 12 nm, which increases its ability to form aggregates and consequently agglomerates.[44,45] In fact, these aggregates are reported to form tortuous mesoporous structures to a higher degree than carbon nanofibers in the static synthesis of ZSM-5.[26] In our case, most of the MWW crystals are formed by platelets with thicknesses of 20−30 nm (8−12 MWW stacked layers each with a thickness of 2.5 nm), which are in an edge-to-face orientation (see Figure S1, image a). In addition, TEM analysis of the MWW crystals (Figure S1, images b,c) did not show intracrystalline mesopores or defects, which confirms that small and tortuous aggregates of BP 2000 limit the interaction of BP 2000 only to the external surfaces of the MWW crystals.

The crystallization of (P)MCM-22-BP was followed by XRD (see Figure S3). On the first day, only a broad reflection between the 2θ range of 15 and 30°, characteristic of an amorphous phase, was observed. Crystallization begins on the second day because of the emergence of intracrystalline (100), (220), and (310) reflection planes, which precedes the stacking of the layers of the basal reflections (002) that appears on the third day. The following days are characterized by growth and crystallization until the seventh day.

To understand the interaction between BP 2000 and the zeolitic structure, Fourier transform infrared (FTIR) analysis of the BP 2000 was carried out and is shown in Figure S4. The

DOI: 10.1021/acsomega.8b00647
ACS Omega 2018, 3, 6217−6223

FTIR results showed a band at 1680 cm^{-1}, which is characteristic of the stretching mode of carbonyl (C═O) groups (aldehyde, ketone, ester, and/or carboxylic acid). Additionally, the signals at 2112, 2627, and 3066 cm^{-1} (broad band) and 3554 cm^{-1} are associated with the stretching modes of alkynyl (C≡C), O−H from carboxylic acid, alkenyl C−H, and phenol O−H groups, respectively.[46] Therefore, the gel precursor is rich in silanol and amino groups derived from HMI as well as Si−O and Al−O bonds, which interact with BP 2000 via hydrogen bonding. Furthermore, it is more probable that silanol groups on the surface of the MWW lamellae are saturated by HMI, which is more basic than any of the functional groups of BP 2000, and consequently, some part of HMI should be replaced by carbon black. Indeed, weight loss values between 180 and 480 °C (see Table 1) confirm that the HMI content in (P)MCM-22-BP was 11% and less than that in traditional (P)MCM-22 (12.3%). Furthermore, TGA analysis of BP 2000 (Figure S4, image b) showed that total oxidation of BP 2000 occurred at 480−800 °C with a maximum loss centering at 580 °C. Indeed, weight loss values above the temperature of 480 °C is referred to oxidation of BP 2000, some remaining HMI molecules, which were not previously oxidized, and dihydroxylation water produced by condensation phenomenon of surface silanol groups. The weight loss value above the temperature of 480 °C was higher for the (P)MCM-22-BP (7.73%) than for the traditional (P)MCM-22 (5.70%). The elemental CHN analyses in Table 1 confirmed the higher C content in (P)MCM-22-BP than in the traditional (P)MCM-22 sample, which is attributed to the presence of BP 2000.

We summarize the formation of dandelion-like microspheres in the scheme shown in Figure 7. BP 2000 was added into the gel solution followed by a slow dropwise addition of colloidal silica. Then, stumbling under hydrothermal conditions proceeded. On the first day, only an amorphous phase was observed, and on the second day, MWW crystallization began. The tortuous shape of the agglomerated BP 2000 and its interaction via hydrogen bonds with the gel precursor where some HMI molecules were replaced by the functional groups of the BP 2000, allowing the growth of MWW crystals in an edge-to-face orientation. On the seventh day, a microsphere with a dandelion-like morphology was obtained.

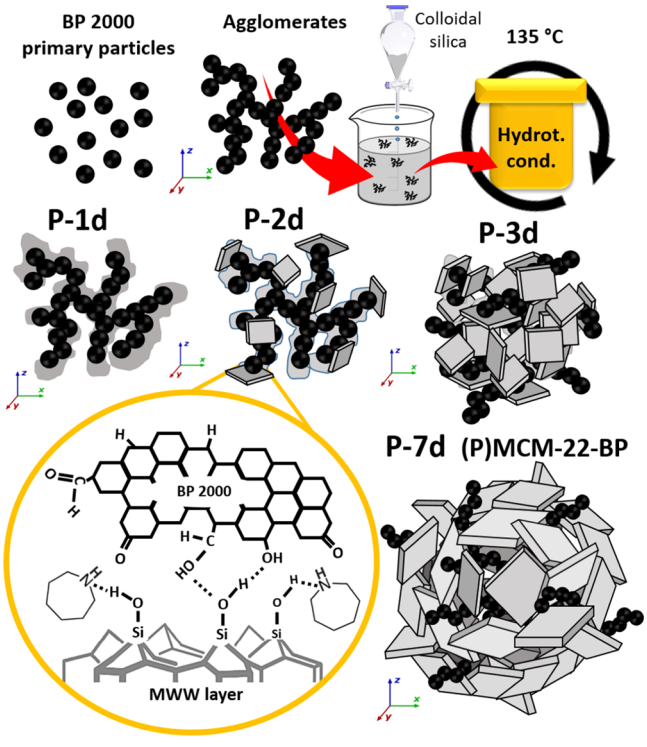

Figure 7. Schematic representation of the precursor formation of the MCM-22-BP dandelion-like microsphere using BP 2000 as a hard template.

CONCLUSIONS

We demonstrate an easy way to integrate intercrystalline macroporosity and morphology control in the MCM-22 zeolite with a one-pot approach using BP 2000 as an inexpensive hard template. It was observed that BP 2000 plays a key role in creating a dandelion-like microspherical morphology for the MCM-22 zeolite. The microspheres were not dense and were composed of MWW crystalline particles in edge-to-face orientations in the entire microspheres. The stacking of the crystals allowed access in several directions to the microsphere interiors. The introduction of BP 2000 as a hard template did not compromise the crystallinity and efficiency of aluminum during nucleation. In addition, the microporous nature was substantially maintained followed by the increase of intercrystalline porosity with larger mesopores and macropores than with traditional MCM-22. These results showed that it is possible to achieve controlled large-sized particles in the MCM-22 zeolite without compromising crystallinity and microporosity. The applications of dandelion-like MCM-22 are currently being explored.

EXPERIMENTAL SECTION

The synthesis of the (P)MCM-22 precursor with a Si/Al = 25 molar ratio was done similar to the literature .[39] Under stirring, 9.25 mmol of sodium hydroxide (NaOH, Sigma-Aldrich) and 4.51 mmol of sodium aluminate ($NaAlO_2$, Riedel-de-Haën) were dissolved in 4.51 mol of distilled water. Then, 50.21 mmol of HMI (Sigma-Aldrich) and carbon black BP 2000 (Cabot) were added into the mixture. The weight ratio between the aluminum used for the synthesis and BP-2000 is 12. After 30 min, 100 mmol of colloidal silica (AS 40, Sigma-Aldrich) was slowly added dropwise into the mixture. The gel was stirred for 2 h and hydrothermally treated in a polytetrafluoroethylene-lined stainless-steel autoclave at 135 °C for 7 days with stumbling (60 rpm). The autoclaved sample was quenched, filtered, washed with distilled water, and dried overnight at 60 °C and was labeled (P)MCM-22-BP. The sample was calcined at 580 °C for 12 h and labeled MCM-22-BP. For the traditional synthesis of the MCM-22 precursor ((P)MCM-22), no BP 2000 was added to the gel composition.

For comparison, the synthesis of the MCM-22 zeolite under static conditions was carried out as described in the previous literature:[47] The Si/Al molar ratio was 25 and 16 days of crystallization at 150 °C. Filtration, drying, and calcination were performed similarly to the previous samples. The material was named MCM-22-static.

CHARACTERIZATION

Powder XRD patterns were collected on a PANalytical Cubix FAST diffractometer using Cu Kα1 radiation and an X'Celerator detector in Bragg−Brentano geometry.

Nitrogen adsorption−desorption isotherms at −196 °C were measured with an Autosorb-1 MP equipment (Quantachrome

DOI: 10.1021/acsomega.8b00647
ACS Omega 2018, 3, 6217−6223

Instruments), and the carbon dioxide adsorption at 0 °C (up to 10 bar) was performed in an ASAP-2050 (Micromeritics). Before the measurements, the samples were outgassed for 12 h at 250 °C. The specific surface area (S_{BET}) was calculated by the BET (Brauer, Emmet and Teller) method from the nitrogen adsorption data in the relative pressure range from 0.007 to 0.04.[48] The V_{TP} was obtained applying the Gurvich rule from the adsorbed amount of N_2 at a relative pressure of 0.98.[49] The external surface area (S_{ext}) and V_{micro} were estimated with the α_S-plot method using N_2 adsorption data and the LiChrospher Si-1000 macroporous silica as reference material. The $V_{micro\text{-}CO_2}$, using CO_2 adsorption data, was estimated by the Dubinin–Radushkevich method. The micropore size distributions were obtained from the CO_2 adsorption data using the Horvath–Kawazoe method. In addition, to study the macropores of the zeolites, their textural characterization was complemented by mercury porosimetry (Autopore III 9410, Micromeritics).

Elemental analysis was determined by an ICP Varian 715-ES ICP optical emission spectrometer after dissolution of the solids in a HNO_3/HF solution. The CHN analysis was performed using a PerkinElmer M CHN Analyzer 2400.

TGA/differential thermal analysis was performed on a Mettler-Toledo TGA/SDTA851E in air flux with a heating range of 10 °C min^{-1}.

FTIR spectrometry was performed by a PerkinElmer instrument, SPECTRUM 65 model, using the attenuated total reflection method, and data were recorded from 4000 to 650 cm^{-1} with a resolution of 1 cm^{-1}.

SEM micrographs were recorded on a ZEISS Ultra 55 microscope operating at 2 kV. TEM analysis was recorded on a Philips CM10 operating at 100 kV.

Solid-state NMR spectra were recorded at room temperature with a Bruker AV 400 spectrometer. ^{27}Al MAS NMR spectra were recorded with a spinning rate of 10 kHz and a 9° pulse length of 0.5 μs with a 1 s repetition time. ^{27}Al chemical shifts were referenced to $Al^{3+}(H_2O)_6$.

■ ASSOCIATED CONTENT

Supporting Information

The Supporting Information is available free of charge on the ACS Publications website at DOI: 10.1021/acsomega.8b00647.

Additional TEM images of dandelion-like MCM-22-BP, nitrogen adsorption and desorption isotherm of MCM-22-static, XRD patterns of (P)MCM-22-BP at different crystallization times, and TGA and FTIR analyses of BP 2000 (PDF)

■ AUTHOR INFORMATION

Corresponding Author

*E-mail: anderson-js@live.com (A.J.S.).

ORCID

Anderson Schwanke: 0000-0002-1273-9940

Urbano Díaz: 0000-0003-1472-8724

Avelino Corma: 0000-0002-2232-3527

Notes

The authors declare no competing financial interest.

■ ACKNOWLEDGMENTS

A.J.S. is grateful to the CAPES Foundation and PDSE program (process number 99999.004779/2014-02) from the Ministry of Education of Brazil. U.D. and A.C. acknowledge funding by the Spanish Government (Severo Ochoa program SEV-2012-0267 and MAT2014-52085-C2-1-P) and the Generalitat Valenciana (Prometeo). The European Union is also acknowledged by ERC-AdG-2014-671093—SynCatMatch. S.P. and K.S. acknowledge the CAPES-CAFP project number 054/14.

■ REFERENCES

(1) Corma, A. From Microporous to Mesoporous Molecular Sieve Materials and Their Use in Catalysis. *Chem. Rev.* **1997**, *97*, 2373–2420.

(2) Shi, J.; Wang, Y.; Yang, W.; Tang, Y.; Xie, Z. Recent advances of pore system construction in zeolite-catalyzed chemical industry processes. *Chem. Soc. Rev.* **2015**, *44*, 8877–8903.

(3) Davis, M. E. Ordered porous materials for emerging applications. *Nature* **2002**, *417*, 813–821.

(4) Mintova, S.; Jaber, M.; Valtchev, V. Nanosized microporous crystals: emerging applications. *Chem. Soc. Rev.* **2015**, *44*, 7207–7233.

(5) Chen, L.-H.; Li, X.-Y.; Rooke, J. C.; Zhang, Y.-H.; Yang, X.-Y.; Tang, Y.; Xiao, F.-S.; Su, B.-L. Hierarchically structured zeolites: synthesis, mass transport properties and applications. *J. Mater. Chem.* **2012**, *22*, 17381–17403.

(6) Schwieger, W.; Machoke, A. G.; Weissenberger, T.; Inayat, A.; Selvam, T.; Klumpp, M.; Inayat, A. Hierarchy concepts: classification and preparation strategies for zeolite containing materials with hierarchical porosity. *Chem. Soc. Rev.* **2016**, *45*, 3353–3376.

(7) Prieto, G.; Tüysüz, H.; Duyckaerts, N.; Knossalla, J.; Wang, G.-H.; Schüth, F. Hollow Nano- and Microstructures as Catalysts. *Chem. Rev.* **2016**, *116*, 14056.

(8) Teng, Z.; Su, X.; Zheng, Y.; Sun, J.; Chen, G.; Tian, C.; Wang, J.; Li, H.; Zhao, Y.; Lu, G. Mesoporous Silica Hollow Spheres with Ordered Radial Mesochannels by a Spontaneous Self-Transformation Approach. *Chem. Mater.* **2013**, *25*, 98–105.

(9) Pagis, C.; Prates, A. R. M.; Farrusseng, D.; Bats, N.; Tuel, A. Hollow Zeolite Structures: An Overview of Synthesis Methods. *Chem. Mater.* **2016**, *28*, 5205–5223.

(10) Chen, Y.; Chen, H.; Guo, L.; He, Q.; Chen, F.; Zhou, J.; Feng, J.; Shi, J. Hollow/Rattle-Type Mesoporous Nanostructures by a Structural Difference-Based Selective Etching Strategy. *ACS Nano* **2010**, *4*, 529–539.

(11) Chen, Y.; Chen, H.; Sun, Y.; Zheng, Y.; Zeng, D.; Li, F.; Zhang, S.; Wang, X.; Zhang, K.; Ma, M.; He, Q.; Zhang, L.; Shi, J. Multifunctional Mesoporous Composite Nanocapsules for Highly Efficient MRI-Guided High-Intensity Focused Ultrasound Cancer Surgery. *Angew. Chem., Int. Ed.* **2011**, *50*, 12505–12509.

(12) Joo, J. B.; Vu, A.; Zhang, Q.; Dahl, M.; Gu, M.; Zaera, F.; Yin, Y. A Sulfated ZrO2 Hollow Nanostructure as an Acid Catalyst in the Dehydration of Fructose to 5-Hydroxymethylfurfural. *ChemSusChem* **2013**, *6*, 2001–2008.

(13) Li, K.; Valla, J.; Garcia-Martinez, J. Realizing the Commercial Potential of Hierarchical Zeolites: New Opportunities in Catalytic Cracking. *ChemCatChem* **2014**, *6*, 46–66.

(14) Prasomsri, T.; Jiao, W.; Weng, S. Z.; Martinez, J. G. Mesostructured zeolites: bridging the gap between zeolites and MCM-41. *Chem. Commun.* **2015**, *51*, 8900–8911.

(15) Inagaki, M.; Toyoda, M.; Soneda, Y.; Tsujimura, S.; Morishita, T. Templated mesoporous carbons: Synthesis and applications. *Carbon* **2016**, *107*, 448–473.

(16) Holland, B. T.; Abrams, L.; Stein, A. Dual Templating of Macroporous Silicates with Zeolitic Microporous Frameworks. *J. Am. Chem. Soc.* **1999**, *121*, 4308–4309.

(17) Xu, L.; Wu, S.; Guan, J.; Wang, H.; Ma, Y.; Song, K.; Xu, H.; Xing, H.; Xu, C.; Wang, Z.; Kan, Q. Synthesis, characterization of hierarchical ZSM-5 zeolite catalyst and its catalytic performance for phenol tert-butylation reaction. *Catal. Commun.* **2008**, *9*, 1272–1276.

(18) Zhang, B.; Davis, S. A.; Mann, S.; Mendelson, N. H. Bacterial templating of zeolite fibres with hierarchical structure. *Chem. Commun.* **2000**, *9*, 781–782.

DOI: 10.1021/acsomega.8b00647
ACS Omega 2018, 3, 6217–6223

(19) Katsuki, H.; Furuta, S.; Watari, T.; Komarneni, S. ZSM-5 zeolite/porous carbon composite: Conventional- and microwave-hydrothermal synthesis from carbonized rice husk. *Microporous Mesoporous Mater.* **2005**, *86*, 145−151.
(20) Liu, Y.; Zhang, W.; Liu, Z.; Xu, S.; Wang, Y.; Xie, Z.; Han, X.; Bao, X. Direct Observation of the Mesopores in ZSM-5 Zeolites with Hierarchical Porous Structures by Laser-Hyperpolarized 129Xe NMR. *J. Phys. Chem. C* **2008**, *112*, 15375−15381.
(21) Wang, Y.; Tang, Y.; Dong, A.; Wang, X.; Ren, N.; Gao, Z. Zeolitization of diatomite to prepare hierarchical porous zeolite materials through a vapor-phase transport process. *J. Mater. Chem.* **2002**, *12*, 1812−1818.
(22) Zhu, H.; Liu, Z.; Wang, Y.; Kong, D.; Yuan, X.; Xie, Z. Nanosized $CaCO_3$ as Hard Template for Creation of Intracrystal Pores within Silicalite-1 Crystal. *Chem. Mater.* **2008**, *20*, 1134−1139.
(23) Machoke, A. G.; Beltrán, A. M.; Inayat, A.; Winter, B.; Weissenberger, T.; Kruse, N.; Güttel, R.; Spiecker, E.; Schwieger, W. Micro/Macroporous System: MFI-Type Zeolite Crystals with Embedded Macropores. *Adv. Mater.* **2015**, *27*, 1066−1070.
(24) Jacobsen, C. J. H.; Madsen, C.; Houzvicka, J.; Schmidt, I.; Carlsson, A. Mesoporous Zeolite Single Crystals. *J. Am. Chem. Soc.* **2000**, *122*, 7116−7117.
(25) Schmidt, I.; Boisen, A.; Gustavsson, E.; Ståhl, K.; Pehrson, S.; Dahl, S.; Carlsson, A.; Jacobsen, C. J. H. Carbon Nanotube Templated Growth of Mesoporous Zeolite Single Crystals. *Chem. Mater.* **2001**, *13*, 4416−4418.
(26) Janssen, A. H.; Schmidt, I.; Jacobsen, C. J. H.; Koster, A. J.; de Jong, K. P. Exploratory study of mesopore templating with carbon during zeolite synthesis. *Microporous Mesoporous Mater.* **2003**, *65*, 59−75.
(27) Yang, Z. X.; Xia, Y. D.; Mokaya, R. Zeolite ZSM-5 with Unique Supermicropores Synthesized Using Mesoporous Carbon as a Template. *Adv. Mater.* **2004**, *16*, 727−732.
(28) Fan, W.; Snyder, M. A.; Kumar, S.; Lee, P.-S.; Yoo, W. C.; McCormick, A. V.; Penn, R. L.; Stein, A.; Tsapatsis, M. Hierarchical nanofabrication of microporous crystals with ordered mesoporosity. *Nat. Mater.* **2008**, *7*, 984−991.
(29) Baughman, R. H.; Zakhidov, A. A.; de Heer, W. A. Carbon Nanotubes−the Route Toward Applications. *Science* **2002**, *297*, 787−792.
(30) Burkat-Dulak, A.; Derewiński, M. Preparation of MFI type zeolite with hierarchical pores system as new supports for deposition of metal clusters. In *Studies in Surface Science and Catalysis*; Antoine Gédéon, P. M., Florence, B., Eds.; Elsevier: Amsterdam, 2008; pp 149−154.
(31) Wei, X.; Smirniotis, P. G. Synthesis and characterization of mesoporous ZSM-12 by using carbon particles. *Microporous Mesoporous Mater.* **2006**, *89*, 170−178.
(32) Kustova, M. Y.; Hasselriis, P.; Christensen, C. H. Mesoporous MEL − Type Zeolite Single Crystal Catalysts. *Catal. Lett.* **2004**, *96*, 205−211.
(33) Jacobsen, C. J. H.; Madsen, C.; Janssens, T. V. W.; Jakobsen, H. J.; Skibsted, J. Zeolites by confined space synthesis − characterization of the acid sites in nanosized ZSM-5 by ammonia desorption and $^{27}Al/^{29}Si$-MAS NMR spectroscopy. *Microporous Mesoporous Mater.* **2000**, *39*, 393−401.
(34) Schmidt, I.; Madsen, C.; Jacobsen, C. J. H. Confined Space Synthesis. A Novel Route to Nanosized Zeolites. *Inorg. Chem.* **2000**, *39*, 2279−2283.
(35) Opanasenko, M. V.; Roth, W. J.; Cejka, J. Two-dimensional zeolites in catalysis: current status and perspectives. *Catal. Sci. Technol.* **2016**, *6*, 2467−2484.
(36) Ramos, F. S. O.; de Pietre, M. K.; Pastore, H. O. Lamellar zeolites: an oxymoron? *RSC Adv.* **2013**, *3*, 2084−2111.
(37) Diaz, U.; Corma, A. Layered zeolitic materials: an approach to designing versatile functional solids. *Dalton Trans.* **2014**, *43*, 10292−10316.
(38) Roth, W. J.; Cejka, J. Two-dimensional zeolites: dream or reality? *Catal. Sci. Technol.* **2011**, *1*, 43−53.
(39) Schwanke, A. J.; Pergher, S.; Díaz, U.; Corma, A. The influence of swelling agents molecular dimensions on lamellar morphology of MWW-type zeolites active for fructose conversion. *Microporous Mesoporous Mater.* **2017**, *254*, 17−27.
(40) Schwanke, A. J.; Díaz, U.; Corma, A.; Pergher, S. Recyclable swelling solutions for friendly preparation of pillared MWW-type zeolites. *Microporous Mesoporous Mater.* **2017**, *253*, 91−95.
(41) Juttu, G. G.; Lobo, R. F. Characterization and catalytic properties of MCM-56 and MCM-22 zeolites. *Microporous Mesoporous Mater.* **2000**, *40*, 9−23.
(42) Cazorla-Amorós, D.; Alcañiz-Monge, J.; de la Casa-Lillo, M. A.; Linares-Solano, A. CO_2 as an adsorptive to characterize carbon molecular sieves and activated carbons. *Langmuir* **1998**, *14*, 4589−4596.
(43) Sing, K. S. W.; Williams, R. T. The Use of Molecular Probes for the Characterization of Nanoporous Adsorbents. *Part. Part. Syst. Char.* **2004**, *21*, 71−79.
(44) Wang, M.-x.; Liu, Q.; Sun, H.-f.; Ogbeifun, N.; Xu, F.; Stach, E. A.; Xie, J. Investigation of carbon corrosion in polymer electrolyte fuel cells using steam etching. *Mater. Chem. Phys.* **2010**, *123*, 761−766.
(45) Wang, Y.-G.; Egashira, M.; Ishida, S.; Korai, Y.; Mochida, I. Microstructure of mesocarbon microbeads prepared from synthetic isotropic naphthalene pitch in the presence of carbon black. *Carbon* **1999**, *37*, 307−314.
(46) University of California, Los Angeles (UCLA). http://webspectra.chem.ucla.edu/irtable.html (Acessed May 07, 2018).
(47) Marques, A. L. S.; Monteiro, J. L. F.; Pastore, H. O. Static crystallization of zeolites MCM-22 and MCM-49. *Microporous Mesoporous Mater.* **1999**, *32*, 131−145.
(48) Brunauer, S.; Emmett, P. H.; Teller, E. Adsorption of Gases in Multimolecular Layers. *J. Am. Chem. Soc.* **1938**, *60*, 309−319.
(49) Sing, K. S. W.; Everett, D. H.; Haul, R. A. W.; Moscou, L.; Pierotti, R. A.; Rouquerol, J.; Siemieniewska, T. Reporting Physisorption Data For Gas/Solid Systems With Special Reference To The Determination Of Surface Area And Porosity. *Pure Appl. Chem.* **1985**, *57*, 603−619.

DOI: 10.1021/acsomega.8b00647
ACS Omega 2018, 3, 6217−6223